A Large Field-of-View Two- and Three-Photon Microscope for High-Resolution Deep Tissue Imaging

Aaron T. Mok,[1,2,*] Tianyu Wang[1], Shitong Zhao[1], Kristine E. Kolkman[3], Danni Wu[4], Dimitre G Ouzounov[1], Changwoo Seo[3,5], Chunyan Wu[1,6,7], Joseph R. Fetcho[3], Chris Xu[1,*]

[1]*School of Applied Engineering Physics, Cornell University, NY, USA*
[2]*Meining School of Biomedical Engineering, Cornell University, NY, USA*
[3]*Department of Neurobiology and Behavior, Cornell University, NY, USA*
[4]*Department of Population Health, New York University, NY, USA*
[5]*Current address: Department of Molecular & Cellular Biology, Harvard University, MA, USA*
[6]*College of Veterinary Medicine, Cornell University, NY, USA*
[7]*Current address: McGovern Institute for Brain Research at MIT, MA, USA*
[*]*tm624@cornell.edu; cx10@cornell.edu*

Abstract

Two-photon microscopy has been engineered to image large populations of neurons in vivo. Three-photon microscopy has achieved a greater imaging depth. However, the attempt to increase its field of view has been hindered by its lower repetition rate. The key to overcoming this challenge is to engineer a scanning scheme that optimized each laser pulse for neuron excitation. We adopted an adaptive excitation scheme that scans solely the region of interest, minimizing wasted excitation pulses. Furthermore, we developed a multi-focus scanning method that increases both scanning speed and laser repetition rate. For the first time, we demonstrated three-photon calcium imaging of neurons within a ~3.5mm diameter field-of-view at a 4Hz frame rate in the deepest cortical layers of mouse brains while preserving high spatial resolution. By reducing the three-photon imaging power, we achieved simultaneous multi-plane imaging with two- and three-photon techniques in both the superficial and deep cortical layers. The demonstrated adaptive scanning module can be integrated into multi-photon microscopes for large-field-of-view imaging, critical for system-level neural circuit research.

Main

High spatial and temporal resolution imaging over a large field-of-view (FOV) deep within intact tissues is valuable for many biological fields such as neuroscience. While large FOV two-photon microscopy (2PM)[1–9] has been successfully demonstrated in recording neural activities up to 5 mm FOV, the penetration depth of two-photon (2P) imaging is limited to 600 to 700 mm in the intact mouse brain [10–12], restricted to the shallow cortical layers. In contrast, three-photon microscopy (3PM) has been shown to reliably image neurons in deep cortical layers[12], subplates[13], and subcortex[14,15]. In addition, a combination of 2PM and 3PM enabled neural imaging in the neocortex and the sub-cortical region simultaneously with a limited FOV[14] of ~ 0.5 x 0.5 mm^2. However, 3PM has a small field of view for high-resolution imaging. The requirement of low laser repetition rates prohibits three-photon microscopy for high-resolution LFOV imaging[10] since the maximum pixel numbers per second cannot exceed the laser repetition rate[14].

We have developed a Dual Excitation with adaptive multi-focus Excitation Polygon-scanning multiphoton microscope (DEEPscope) that enables high-resolution imaging with a large FOV (3.5 mm diameter) deep in scattering tissue. High-resolution imaging is essential to minimize the risk of misattributing calcium transients[16] by reducing the overlap between cells. Figure 1 shows the experimental setup. The microscope allows simultaneous 2P and three-photon (3P) excitation (i.e., dual excitation). The 3P excitation path consists of an adaptive excitation module, a beamlet generation delay line, and a scan engine with a polygon scanner. The 2P excitation path consists of an adaptive excitation module, a remote focusing module, and the same polygon scan engine for 3P excitation. The DEEPscope achieved deep and large FOV imaging in scattering brain tissues by (1) performing fast and large-angle optical scans using the polygon scanner, (2) reducing the power required for large-FOV imaging using adaptive excitation, and (3) improving the excitation efficiency and scanning speed using optimized PSF and beamlets.

While polygon-scanning multiphoton microscopes have been demonstrated before, the FOV is relatively small (~ 512 x 512 mm)[17,18]. We used a polygon scanner to achieve a large scan angle at high scanning speed, which also reduces the complexity of the scanning engine when compared to the existing large FOV microscopes[1,4,7]. The optical path and the footprint for the DEEPscope (~3 ft x 3 ft x 1 ft, Supplementary Fig. 1) are nearly identical to a conventional multiphoton microscope. The polygon scanner has a larger aperture (9.5 mm) and more than twice the optical scan angle (~60-degree peak-to-peak) than a resonant scanner. The polygon line rate (~6 kHz) is > 6 times that of galvo scanners (< 1 kHz) at the same scan angle with ~5 mm aperture size.

To reduce the average power required for simultaneous large FOV 2P and 3P imaging, an adaptive excitation scheme[19] enabled by electro-optical modulators (EOMs) was used to block the laser in areas where large blood vessel shadows were located. Figure 1d shows an image of cortical layer 6 (L6) with and without adaptive excitation. Fluorescence intensity increased during adaptive excitation because the effective power across the regions imaged was higher (224 mW versus 130 mW) even though the average power was lower (119 mW versus 130 mW).

To optimize excitation efficiency and improve imaging speed using a low repetition rate laser, we employed a beamlet scanning scheme with a point spread function (PSF) optimized to the size of neurons. A higher excitation efficiency improves the detection fidelity of calcium transients (d')[20]. We underfilled the back aperture of the DEEPscope objective (~85% filled). The axial resolution across the FOV was ~5 mm full-width half maximum (FWHM) (Supplementary Fig. 2). This size of the PSF is close to the optimum for the size of neuron cell bodies, and approximately doubled d' value by increasing the fluorescence signal ~ 4 times when compared to a PSF with 2-mm axial resolution (Supplementary Fig. 3). This result is consistent with other studies[14]. In addition, we created a beamlet scanning scheme in which two pulses were scanned in two adjacent lines with a time delay of ~20 ns (Fig. 1c). Compared to scanning with a PSF with 10-mm axial resolution, such a two-beamlet scanning scheme with two 5-mm axial resolution PSF further increased d' value by ~10% (fluorescence signal by ~20%) using the same amount of total pulse energy at the focal plane. Furthermore, the beamlets doubled the effective laser repetition rate and the line scanning speed, resulting in doubling both the spatial and the temporal resolution. More beamlets

can be advantageous if higher pulse energy from the excitation source is available, providing greater gains in d' value and higher spatial and temporal resolution (Supplementary Fig. 3).

We performed 3P large FOV structural imaging of neurons in a cortical column and the stratum pyramidale (SP) layer of the CA1 region of the hippocampus in a transgenic mouse (Fig. 2 and Supplementary Video 1). We scanned a 3.23 mm x 3.23 mm field to cover most of the 3.5 mm diameter FOV of the microscope. We imaged a stack from 100 to 1,048 mm in depth (Fig. 2a and Supplementary Video 2). GCaMP6s-expressing neurons in the SP layer appear at ~ 872 mm depth (Fig. 2b). The external capsule (EC), where myelinated axons produce strong third harmonic generation (THG) signals, appeared to be curved across the large FOV and extended from ~600 mm to 1,048 mm below the brain surface (Fig. 2b). After the image acquisition, the digitally zoomed-in images and video (Fig.2b, Fig.2c, Supplementary Video 1 and Supplementary Video 2) show the labeled neurons with clear nuclear exclusion. We also measured an axial resolution of ~5 mm in a vasculature-labeled mouse at a depth of 800 mm below the brain surface (Supplementary Fig. 4). Figure 2 shows that 3P DEEPscope is capable of high-resolution, large FOV imaging deep within intact mouse brains.

We imaged the spontaneous activity of GCaMP6s-expressing neurons in adult transgenic mice in the cortical L6 to demonstrate the capability of the 3P DEEPscope for large FOV activity imaging in the deep cortical regions. Figure 3a shows the 3.23 mm x 3.23 mm scanned field and the digitally zoomed-in imaging sites in cortical L6 at 600 mm depth, right above the EC. We used adaptive excitation to reduce the average excitation power from 224 mW to 119 mW while keeping the same pulse energy at the sample. We recorded neuronal activity traces from a large population of neurons (918 neurons) in an awake mouse (Fig. 3b and Supplementary Video 3) at a 4 Hz frame rate. Figure 3c shows selected activity traces of the neurons. The raw photon counts of the activity recording are shown in Supplementary Fig. 5. We also imaged hippocampal SP neurons at 930 mm depth with a FOV of 550 mm x 550 mm. The FOV for hippocampal imaging was reduced due to the limit on laser average power to prevent tissue heating (Supplementary Fig. 6 and Supplementary Video 4).

While 3P DEEPscope enables deep imaging in mice, 2P imaging achieves a higher volumetric imaging rate for shallow imaging depths due to its higher excitation repetition rate[10]. Therefore, we designed the DEEPscope for excitation wavelengths of 910-930 nm, 1,030-1,050 nm, 1,240-1,380 nm, and 1,640-1,750 nm to enable both 2P shallow and 3P deep imaging. Supplementary Fig. 7 and Supplementary Fig. 8 show the transmission over the entire FOV for 920 nm and 1320 nm. Supplementary Fig. 9a shows an imaging site of L5 neurons 480 mm below the brain surface in an adult transgenic mouse. We recorded the neuronal activity traces of a large population of 2,000 neurons under awake conditions at a ~ 6 Hz frame rate. By reducing the FOV to ~ 3.23 mm x 1 mm, we performed high spatial-resolution activity imaging (0.67 mm pixel size) at a 4 Hz frame rate (Supplementary Fig. 9b). Labeled neurons display clear nuclear exclusion. We recorded the neuronal activity traces of 503 neurons, which demonstrates that the DEEPscope can achieve high speed, large FOV, and high-resolution imaging.

We performed simultaneous six-plane 2P and 3P activity imaging of both shallow and deep cortical GCaMP6s-expressing neurons in adult transgenic mice. Fig. 3d shows 3.23 mm x 3.23

mm FOV 2P imaging of five focal planes at 320, 340, 360, 380, 400 mm depth at a cycling rate of 2.2 Hz and 3P imaging at 600 mm depth at a frame rate of 11 Hz. We were able to record neuronal activity traces from a large population of neurons (4,523 neurons) under awake conditions.

The DEEPscope can be applied to other animal models as well. We performed 3P large FOV imaging of an adult zebrafish brain in vivo[21]. We imaged a stack from 0 to 1,090 mm in depth (Supplementary Fig. 10, Supplementary Videos 5, 6). Individual GCaMP6s-expressing nuclei were clearly visible in the telencephalic, optic tectum, and cerebellar regions and the THG signal revealed bone structures and fiber tracts. The entire olfactory bulbs, the olfactory nerves, and part of the olfactory epithelium were also visible.

The Imaging depth, FOV, and speed are ultimately limited by the achievable fluorescence signal. The adaptive excitation used here by simply blocking the lasers with EOMs in the uninformative parts of the sample suggests that there is room to further increase the excitation efficiency. A customized adaptive excitation source (AES), for example, illuminates the neurons with a high instantaneous repetition rate. It can increase the fluorescence signal by more than 10-fold without increasing the average power as shown in a previous paper[19]. New transgenic mice with brighter jGCaMP7s or jGCaMP8s indicators will further increase fluorescence signal by > 4-fold [22–24] for single and multiple action potentials. The combination of the DEEPscope, the AES, and brighter calcium indicators will further improve the capability for deep, fast, and large FOV imaging of neuronal activity.

Using commercially available 3P and 2P laser systems, a polygon scanner, and EOMs, we have demonstrated a number of practical techniques to significantly improve data quality and throughput for both 2P and 3P imaging systems. By employing adaptive excitation, we can increase the number of recorded neurons without increasing the average power. By generating spatially dispersed beamlets, we can also enhance the scanning rate beyond the limits of the scanners while preserving high spatial resolution, strong multiphoton signal, and a large scanning FOV. The combination of high imaging speed and large volume offered by the DEEPscope will allow simultaneous monitoring of the dynamics of a large population of cells across a large FOV in different kinds of tissues.

METHOD

Dual Excitation with adaptive Excitation Polygon-scanning multiphoton microscope (DEEPscope)

Excitation source and adaptive excitation. The excitation source for 3PM was a noncollinear optical parametric amplifier (NOPA, Spectra-Physics) pumped by an amplifier (Spirit, Spectra-Physics). The NOPA operated at a center wavelength of 1320 nm and provided an average power of ~2 W at 2 MHz repetition rate (~1 mJ per pulse). It was paired with an electro-optic modulator (EOM) (360-80-03, Conoptics) for adaptive excitation[19]. A two-prism (SF11 glass) compressor was used to compensate for the normal dispersion of the optics in the light source and the microscope. The pulse duration (measured by second-order interferometric autocorrelation) under the objective was ~60 fs after dispersion compensation.

The excitation source for 2PM was a mode-locked Ti:Sapphire laser (Chameleon, Coherent). The Ti:Sapphire laser operated at a center wavelength of 920 nm and provided an average power of ~1.6 W at 80 MHz repetition rate. It was paired with an EOM (350-160, Conoptics) for adaptive excitation. A two-prism (SF11 glass) compressor was used to compensate for the normal dispersion of the optics in the light source and the microscope. The pulse duration (measured by second-order interferometric autocorrelation) under the objective was ~90 fs after dispersion compensation.

Beamlet generation delay line. A beamlet generation delay line (Fig. 1) was used to split a laser pulse at 1320 nm into two pulses (beamlets) with ~ 20 ns time delay, increasing the effective laser repetition rate from 2 MHz to 4 MHz. The delay line was arranged as a loop with four one-inch dielectric mirrors (102077, Layertec) and a polarizing beam splitter cube (PBS) (PBS103, Thorlabs). The PBS served as the input and output port of the delay line. The power distribution of each beamlet was controlled by adjusting the half-wave plate (HWP) (WPH05M-1310, Thorlabs) before the PBS. Inside the loop, two mirrors were tilted to adjust the angular separation between the beamlets. The angularly separated beamlets converge on the polygon scanner in a plane that was perpendicular to the scanning direction. An 8-f system was placed inside the loop to compensate for the difference in beam divergence between the beamlets. Two co-planar foci that were ~ 3 mm apart were created along the slow axis (Supplementary Fig. 11). The fluorescence signal generated by the two beamlets is demultiplexed temporally and forms the pixels in the corresponding lines in the image. The crosstalk of the fluorescence signals between the two beamlets was measured to be ~5%, which was caused by the data acquisition bandwidth of the system (Supplementary Fig. 12).

DEEPscope setup. We developed a multiphoton microscope that enables 3.5 mm diameter large FOV imaging (Supplementary Fig. 13) using a custom-designed scan lens (f = 60 mm), tube lens (f = 200 mm), and objective lens (f = 15 mm) (Special Optics, Navitar). The objective lens is water immersion and has a maximum excitation numerical aperture (NA) of 0.75 and a collection NA of 1.0 (Supplementary Fig. 14) with a 2.8 mm working distance. The objective was underfilled with $1/e^2$ beam diameter of ~17 mm to achieve an axial resolution (FWHM) of ~5 *m*m and lateral resolution (FWHM) of ~0.7 *m*m across the FOV (Supplementary Fig. 2 and Supplementary Fig.11) for both 2P excitation at 920 nm and 3P excitation at 1320 nm. A 9-mm aperture polygon scanner and a 10-mm aperture galvo-mirror (Saturn 9B, ScannerMax) were conjugated using two custom-designed scan lenses (f = 60 mm) (Special Optics, Navitar) (Fig. 1). The customized polygon scanner (PT60SRG, Nidec Copal Electronics) has 12 facets, each with 17.5 mm x 9.5 mm clear aperture. Since beam truncation occurs at the edge of each facet, the fill fraction of the polygon scan was 70% both temporally and spatially to ensure uniform transmission across the field of view. A 42-degree peak-to-peak optical scan angle was used to achieve a 3.23 mm linear scan field. The polygon scanner we used is capable of scanning a 60-degree peak-to-peak optical angle with a variable rotation speed of 7,000 – 30,000 revolutions per minute (RPM), i.e., 1.4 kHz – 6 kHz line rate. Polygon scanner with even higher rotation speed, e.g., 55,000 RPM, is possible from different manufacturers, potentially further increasing the scan speed to an 11 kHz line rate.

For hippocampus activity imaging (Supplementary Fig. 6), a 5 mm-aperture non-conjugated galvo-galvo scanner (Saturn 9B, ScannerMax) was used since the FOV was small. This configuration shared the same lenses and effective excitation NA (Supplementary Fig. 2) as the polygon-galvo configuration. The galvo-galvo scanner could achieve ~1 kHz line rate at ~40-degree peak-to-peak optical scan angle.

A fast remote focusing module (Fig. 1) enabled tunning of the 2P focal plane away from the 3P focal plane. In the 2P beam path, an HWP (WPH05M-915, Thorlabs) and PBS (PBS255, Thorlabs) directed the beam onto a quarter wave plate (QWP) and the remote focusing objective (ROBJ) (LMH-50X-850, Thorlabs). The QWP and ROBJ were double passed after reflection from a small mirror (PF03-03-P01) and a custom-made adapter (~20g total weight), which were mounted on a voice coil (LFA 2010; Equipment Solutions). The back aperture of the ROBJ was conjugated to the back aperture of the imaging objective. The axial resolution at different focal plane positions during remote focusing is shown in Supplementary Figure 15.

For signal collection, the fluorescence and third harmonic generation (THG) signal were epi-collected through the imaging objective lens and immediately reflected by a 77 mm x 108 mm dichroic beam splitter (FF705-Di01, Semrock) to a detection system (Special Optics, Navitar) that was custom-designed to achieve a high collection efficiency. Another 77 mm x 108 mm dichroic mirror (FF470-Di01, Semrock) split the signal into two channels: one for the fluorescence signal emitted from GCaMP6s and the other for the THG signal. One-inch optical filters 520/70 (FF01-520/70, Semrock) and 435/40 (FF02-435/40, Semrock) were used for the fluorescence and THG channels, respectively. The signals were detected with two 14x14 mm^2 effective sensor area GaAsP photomultiplier tube (H15460-40) that was customized for low dark-count and with the built-in preamplification unit removed. The detection efficiency of the system was estimated to be ~3.5% for fluorescence imaging across the 3.5 mm FOV at an imaging depth of 900 μm (using an established empirical model[25] and the measurement result in Supplementary Fig. 14).

The PMT current was converted to voltage by a transimpedance amplifier **(**HCA-200M-20K-C, Femto). Analog-to-digital conversion was done by a data acquisition card at a sampling clock of 123 MHz (vDAQ, Vidrio), triggered by the Spirit-NOPA system at 1.96 MHz with a 63x electronic multiplier. Light shielding was carefully done to achieve a dark count of ~1000 photons per second under the usual imaging environment. The acquisition system achieved shot-noise-limited performance. 3P signals for the two beamlets were acquired with two acquisition gates for time demultiplexing. A customized ScanImage 2021 (Vidrio) running on Matlab (MathWorks) was used to place the 3P signals from each beamlet into two virtual channels. These channels were interleaved with a custom Matlab script after image acquisition. 2P signal was placed into a separate virtual channel. A translation stage was used to move the sample (M-285, Shutter Instrument). For depth measurement, the slightly larger index of refraction in brain tissue relative to water resulted in a slight underestimate (5–10%) of the actual imaging depth within the tissue, because the imaging depths reported here are the raw axial movement of the sample[26].

Two-photon and three-photon temporal multiplexing. Simultaneous 2P and 3P excitation were achieved by temporal multiplexing of the 920 nm Ti:Sapphire laser and the 1320 nm Spirit-NOPA. The setup is similar to the one described in a previous study[15]. Briefly, the two excitation beams

were combined with a 980 nm long pass dichroic mirror (DMLP1000R, Thorlabs) and passed through the same scanners. They were spatially separated into different focal planes by using the remote focusing module. The 920 nm laser was intensity modulated with an EOM, which was controlled by a transistor-transistor logic (TTL) gate signal. The TTL signal was generated from a signal generator (SDG2042X, Siglent) that was triggered by the Spirit-NOPA laser. The EOM had high transmission for 360 ns between two adjacent Spirit-NOPA laser pulses (or pulse pairs for the two beamlets) that were ~ 500 ns apart.

Adaptive excitation. A structural image was first obtained from conventional raster scanning. Then Gaussian filters and median filters were used to remove sharp features in the image. The regions for imaging were selected by using the top 80% of pixel intensity in the structural image, which effectively excludes regions of the blood vessel shadows. The positions of the areas for imaging were then converted into a digital time sequence for each scan line and sent to an arbitrary waveform generator (AWG). The AWG, triggered by the line trigger from ScanImage, controlled a Pockels cell to transmit laser power only to the selected areas within the FOV.

Adaptive excitation for 3PE was achieved with one AWG (PXI-5412, National Instrument). Adaptive excitation for 2P/3P multiplexing was achieved with two AWGs (PXI-5421 and PXI-5412, National Instrument) to accommodate different selected areas at different imaging depths. The AWGs were configured to have a sampling rate of 5 MHz. For 3PM, the time sequence from the AWG was directly sent to the Pockels cell driver (302A, Conoptics). For 2PM, the time sequence from the AWG was combined with the TTL gate signal (see the section on *Two-photon and three-photon temporal multiplexing*) with an AND gate (TI SN74HC08N, Texas Instruments) before sending it to the Pockels cell driver (25D, Conoptics) (Supplementary Fig. 16).

Image acquisition parameters. All acquisition parameters for structural and functional imaging are summarized in Supplementary Table 1.

Image processing for structural recording

Structural imaging was normalized by the linear transform of pixel intensities to saturate the brightest 0.1-0.5% pixels in each frame. Three-dimensional reconstruction of the stacks was rendered in Imaris.

Image processing and data analysis for activity recording

Motion corrections were performed using Suite2p[27]. Neuron segmentation was done using Suite2p or manually with ImageJ. Extractions of fluorescence time traces (F) were done with Suite2p or a custom Matlab script.

In Matlab, traces (F) were filtered with a moving average of window size of 2s. Baselines of the traces (F_0) were determined by excluding the spikes and their rising and falling edges. Traces (F) were normalized according to the formula $(F-F_0)/F_0$.

For the visual representation of calcium activities in Supplementary Video 3, the raw image sequence was processed by Kalman filter with a gain of 0.7. For Supplementary Video 4, the raw

image sequence was processed by moving average of 4 frames and Kalman filter with a gain of 0.8 (left) and by DeepCAD[28] (right).

Excitation efficiency optimization using discriminability index (d')

The discriminability index (d') for calcium transient detection using the beamlet scanning schemes (Supplementary Fig. 3) was calculated according to equations for three-photon excited fluorescence in a Gaussian focus[11,29]. All calculations were performed assuming a spherical region of interest (ROI) with a radius of 5 mm. Excitation inside the ROI yields a fluorescence signal while excitation outside the ROI yields background. To maximize power efficiency, we assumed 100% labeling density to penalize excitation outside the ROI and to reduce neuropil contamination. The refractive index of the medium was 1.33. The center wavelength was 1320 nm and the laser pulse width was 60 fs (FWHM). Three-photon cross-section of GCaMP6s (3×10^{-82} cm^6s^2) was used to calculate the fluorescence signal and the saturation pulse energy.

Animal surgery and *in-vivo* calcium imaging of awake mice

All animal experiments and housing procedures were conducted in accordance with Cornell University Institutional Animal Care and Use Committee guidance. Chronic craniotomy was performed on mice according to the procedures described in the previous work[15]. Briefly, a window of 5 mm diameter was created, centering at ~2.5 mm lateral and ~2 mm caudal from the bregma point over the somatosensory cortex. Calcium imaging was performed on transgenic animals with GCaMP6s-expressing neurons (male and female, 15-18 weeks, *CamKII-tTA/tetO-GCaMP6s*). The spontaneous calcium activity imaging was performed on awake animals. The imaging took place 2-8 weeks after cranial window implantation.

Vasculature imaging for resolution measurement

The mice were anesthetized with isoflurane (1–1.5% in oxygen, with breathing frequency maintained at 1 Hz) and placed on a heat blanket to maintain body temperature at 37.5 °C. Eye ointment was applied. The vasculature of the transgenic mouse (*TIT2L-GC6s-ICL-tTA2*, female, 25 weeks) was labeled via retro-orbital injection of fluorescein (25 mg of dextran conjugate dissolved in 200 mL of sterile saline, 70-kDa molecular weight; D1823, Invitrogen).

Animal surgery and in vivo calcium imaging of zebrafish

Adult zebrafish (*Danio rerio*) (*Tg(elavl3::H2B-GCaMP6s*), male, 9 months postfertilization[30] were used. Small to medium-sized fish were chosen (standard lengths (tip of the head to the base of tail) 15.4 mm) for whole brain imaging. Zebrafish were anesthetized with 0.2 mg mL^{-1} tricaine solution (pH 7.2). Then, 2 mL pancuronium bromide (0.4 mg mL^{-1} in Hanks) was retro-orbitally injected to paralyze the fish. The fish was then transferred to a petri dish with a 'V'-shaped mounting putty (Loctite) to support the fish with the dorsal side up. A drop of the anesthetic bupivacaine was placed on the head. A small strip of putty was gently placed over the back of the fish to secure it. Fish were perfused through the mouth with an ESI MP2 Peristaltic Pump (Elemental Scientific) at a rate of 2 mL min^{-1} with oxygenated fish system water during the experiment.

Acknowledgments

We thank members of the Xu research group, especially Bo Li, Xusan Yang, and Kibaek Choe for their help and valuable discussions. We thank Spencer Smith and Che-Hang Yu for the discussion of optics design. We thank Katherine Strednak, Emily Silvela, and Faith Burgus from Cornell Center for Animal Resources and Education for their animal care service. We thank Karl Termini from the Cornell glass shop for his help in glass grinding. We thank Robert Page, Stanley McFall, Chris Cowulich, and Jeffrey Koski from the Cornell machine shop for their help in machining. We thank the Cornell Institute of Biotechnology for providing a workstation for 3D rendering. We thank Vidrio, Special Optics, Nidec Copal Electronics, Hamamatsu Photonics, ScannerMax, Eksma Optics, and AVR optics for customized parts. This research was supported by the National Science Foundation NeuroNex (grant no. DBI-1707312 to C.X.) and partially funded by NIH/NINDS (grant no. U01NS103516 to C.X.) and Cornell Neurotech Mong Fellowship.

Author information

Contributions

A.M., T.W., and C.X. conceived the study. A.M. designed, built, and maintained the imaging system. A.M. designed, performed the experiments, and analyzed the results. T.W. designed the imaging system, performed and discussed data analysis. S. Z. built the adaptive excitation system. K.E.K. and J.F. prepared Zebrafish samples, performed and discussed data analysis. D.W. performed data analysis. D.G.O. maintained the laser system. C.S. designed and discussed animal setup and preparation. C.W. discussed animal preparation. C.X. supervised the research. A.M. and C.X. wrote the manuscript.

Ethics declarations

Competing interests

C.X., A.M., T.W., are listed as inventors on a US provisional patent application (serial no. 63/464,489) on Optical Pulse Generator and Method. The other authors declare no competing interests.

References

1. Sofroniew, N. J., Flickinger, D., King, J. & Svoboda, K. A large field of view two-photon mesoscope with subcellular resolution for in vivo imaging. *eLife* **5**, e14472 (2016).

2. Lu, R. *et al.* Rapid mesoscale volumetric imaging of neural activity with synaptic resolution. *Nature Methods* **17**, 291–294 (2020).

3. Demas, J. *et al.* High-speed, cortex-wide volumetric recording of neuroactivity at cellular resolution using light beads microscopy. *Nature Methods* **18**, 1103–1111 (2021).

4. Stirman, J. N., Smith, I. T., Kudenov, M. W. & Smith, S. L. Wide field-of-view, multi-region, two-photon imaging of neuronal activity in the mammalian brain. *Nature Biotechnology* **34**, 857–862 (2016).

5. Yu, C.-H., Stirman, J. N., Yu, Y., Hira, R. & Smith, S. L. Diesel2p mesoscope with dual independent scan engines for flexible capture of dynamics in distributed neural circuitry. *Nature Communications* **12**, 1–13 (2021).

6. Clough, M. *et al.* Flexible simultaneous mesoscale two-photon imaging of neural activity at high speeds. *Nature Communications* **12**, 1–7 (2021).

7. Ota, K. *et al.* Fast, cell-resolution, contiguous-wide two-photon imaging to reveal functional network architectures across multi-modal cortical areas. *Neuron* **109**, 1–15 (2021).

8. Rumyantsev, O. I. *et al.* Fundamental bounds on the fidelity of sensory cortical coding. *Nature* **580**, 100–105 (2020).

9. Tsai, P. S. *et al.* Ultra-large field-of-view two-photon microscopy. *Optics Express* **23**, 13833–13847 (2015).

10. Wang, T. & Xu, C. Three-photon neuronal imaging in deep mouse brain. *Optica* **7**, 947–960 (2020).

11. Wang, T. *et al.* Quantitative analysis of 1300-nm three-photon calcium imaging in the mouse brain. *eLife* **9**, e53205 (2020).

12. Takasaki, K., Abbasi-asl, R. & Waters, J. Superficial bound of the depth limit of two- photon imaging in mouse brain. *eNeuro* **7**, 1–10 (2020).

13. Yildirim, M., Sugihara, H., So, P. T. C. & Sur, M. Functional imaging of visual cortical layers and subplate in awake mice with optimized three-photon microscopy. *Nature Communications* **10**, 177 (2019).

14. Weisenburger, S. *et al.* Volumetric Ca2+ imaging in the mouse brain using hybrid multiplexed sculpted light microscopy. *Cell* **177**, 1–17 (2019).

15. Ouzounov, D. G. *et al.* In vivo three-photon imaging of activity of GCaMP6-labeled neurons deep in intact mouse brain. *Nature Methods* **14**, 388–390 (2017).

16. Gauthier, J. L. *et al.* Detecting and correcting false transients in calcium imaging. *Nature Methods* **19**, 470–478 (2022).

17. Li, Y. *et al.* High contrast imaging and flexible photomanipulation for quantitative in vivo multiphoton imaging with polygon scanning microscope. *Journal of Biophotonics* **11**, 1–12 (2018).

18. Li, Y. X. *et al.* Flexible polygon-mirror based laser scanning microscope platform for multiphoton in-vivo imaging. *Journal of Biophotonics* **10**, 1526–1537 (2017).

19. Li, B., Wu, C., Wang, M., Charan, K. & Xu, C. An adaptive excitation source for high-speed multiphoton microscopy. *Nature Methods* **17**, 163–166 (2020).

20. Wilt, B. A., Fitzgerald, J. E. & Schnitzer, M. J. Photon shot noise limits on optical detection of neuronal spikes and estimation of spike timing. *Biophysical Journal* **104**, 51–62 (2013).

21. Chow, D. M. *et al.* Deep three-photon imaging of the brain in intact adult zebrafish. *Nature Methods* **17**, 605–608 (2020).

392 22. Bounds, H. A. *et al.* Ultra-precise all-optical manipulation of neural circuits with multifunctional
393 Cre-dependent transgenic mice. *bioRxiv* (2022) doi:10.1101/2021.10.05.463223.

394 23. Dana, H. *et al.* High-performance calcium sensors for imaging activity in neuronal populations
395 and microcompartments. *Nature Methods* **16**, 649–657 (2019).

396 24. Zhang, Y. *et al.* Fast and sensitive GCaMP calcium indicators for imaging neural populations.
397 *bioRxiv* (2021) doi:10.1101/2021.11.08.467793.

398 25. Beaurepaire, E. & Mertz, J. Epifluorescence collection in two-photon microscopy. *Applied Optics*
399 **41**, 5376–5382 (2002).

400 26. Wang, T. *et al.* Three-photon imaging of mouse brain structure and function through the intact
401 skull. *Nature Methods* **15**, 789–792 (2018).

402 27. Pachitariu, M. *et al.* Suite2p: beyond 10,000 neurons with standard two-photon microscopy.
403 *bioRxiv* (2017) doi:10.1101/061507.

404 28. Li, X. *et al.* Reinforcing neuron extraction and spike inference in calcium imaging using deep self-
405 supervised denoising. *Nature Methods* **18**, 1395–1400 (2021).

406 29. Xu, C. & Webb, W. W. Multiphoton Excitation of Molecular Fluorophores and Nonlinear Laser
407 Microscopy. in *Topics in Fluorescence Spectroscopy* (ed. Lakowicz, J. R.) vol. 5 471–540
408 (Springer, Boston, MA, 2002).

409 30. Vladimirov, N. *et al.* Light-sheet functional imaging in fictively behaving zebrafish. *Nature*
410 *Methods* **11**, 883–884 (2014).

411

412

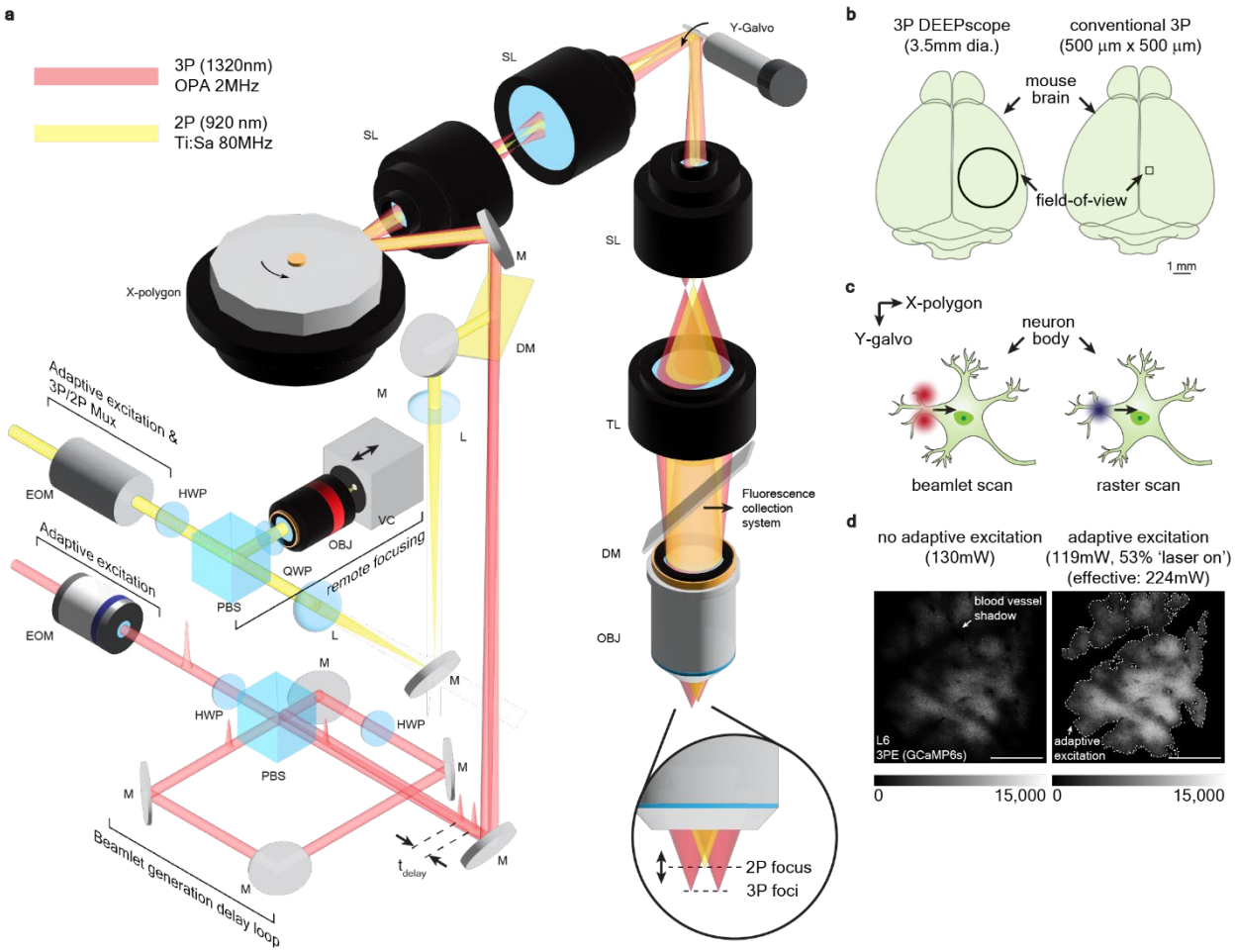

Figure 1. Dual-beam Excitation with adaptive Excitation Polygon-scanning multiphoton microscope (DEEPscope). (a) DEEPscope schematics. The 3P path consists of an adaptive excitation module, a beamlet generation delay loop, and a scan engine with a polygon scanner. The 2P path consists of an adaptive excitation module, a 3P/2P multiplexing module, a remote focusing module, and the same scan engine as for 3P imaging. (**b)** Comparison of the field-of-view (FOV) of 3P DEEPscope with conventional 3P microscopes. DEEPscope images 3.5 mm diameter FOV in the mouse brain. **(c)** Schematic of beamlet scanning with the beamlet generation delay loop. (**d)** Comparison of fluorescence intensity across the FOV with and without adaptive excitation at similar average excitation power. Grayscale bar shows pixel intensity. Scale bar, 1 mm. EOM: electro-optic modulator, HWP: half-wave plate, QWP: quarter wave-plate, PBS: polarization beam splitter, L: lens, M: mirror, SL: scan lens, TL: tube lens, DM: dichroic mirror, OBJ: objective, t_{delay}: time delay between the pulses of the two beamlets.

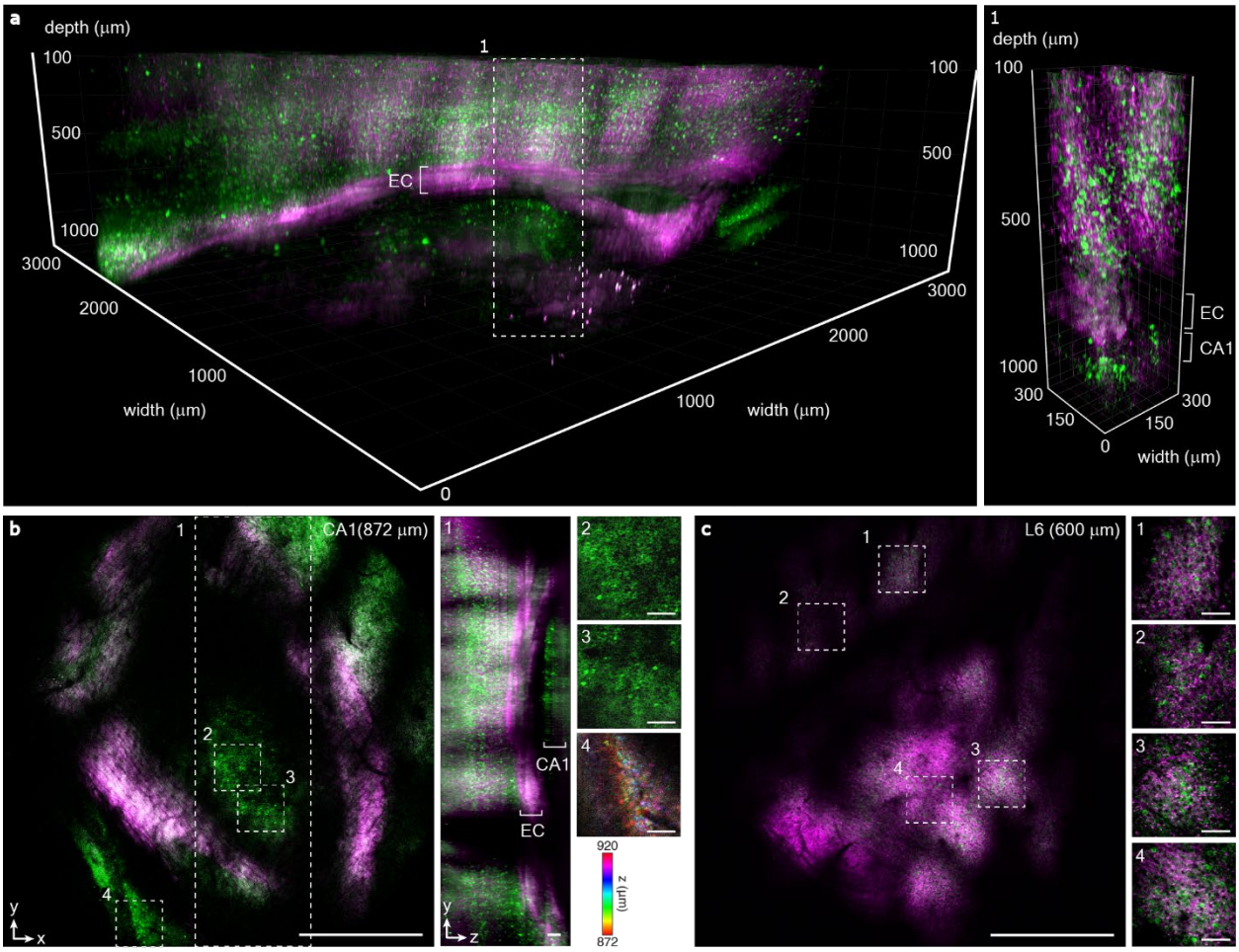

Figure 2. Deep and large FOV *in-vivo* imaging of mouse brain structures. (**a)** 3D rendering of GCaMP6s-expressing neurons by 3P DEEPscope from 100 to 1,048 mm below the brain surface (*CamKII-tTa/tetO-GCaMP6s mouse*, male, 16 weeks old). The scanning field was ~3.23 mm x 3.23 mm, acquired with 0.8- mm pixel size and a z-step of 4 mm. The integration time per imaging depth was 1.5 mins, 4 mins, and 10 mins at the depth of 100-900 mm, 900-950 mm, and 950-1,048 mm respectively. Panel 1 shows the digitally zoomed-in volume of the 3D stack in **a** (indicated by the white dashed box) with 300 mm FOV. **(b)** Selected 2D images from **a** of CA1 hippocampal neurons at an imaging depth of 872 mm. Panel 1 shows the YZ maximum intensity projection of the dashed box 1 in **b**. Panels 2 to 4 show digitally zoomed-in images of the corresponding white dashed boxes in **b**. Scale bar in **b**, 1 mm. Scale bars in panels 1 to 4, 100 mm. **(c)** Selected 2D image from **a** of layer 6 neurons at an imaging depth of 600 mm. Panels 1-4 show digitally zoomed-in images of the corresponding dashed white boxes in **c**. Scale bar of c, 1 mm. Scale bars in panels 1 to 4, 100 mm. EC: external capsule.

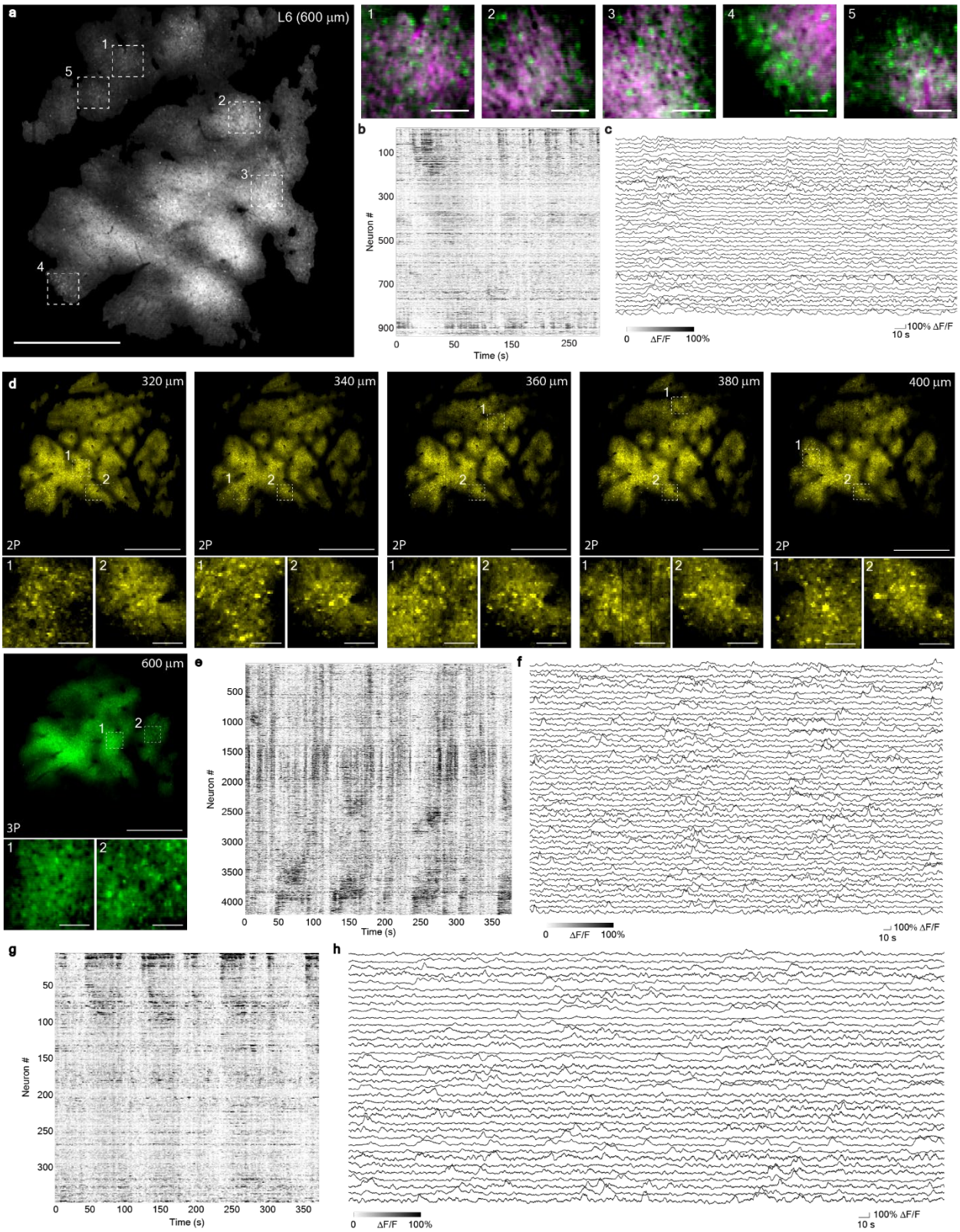
a
L6 (600 µm)
1
2
3
4
5
b
Neuron #
Time (s)
c
0 ΔF/F 100%
100% ΔF/F
10 s
d
320 µm
340 µm
360 µm
380 µm
400 µm
2P
600 µm
3P
e
Neuron #
Time (s)
f
0 ΔF/F 100%
100% ΔF/F
10 s
g
Neuron #
Time (s)
h
0 ΔF/F 100%
100% ΔF/F
10 s

442

443

Figure 3. Large FOV neuronal activity recording in the shallow and deep cortex of GCaMP6s-expressing transgenic mouse. (a) 3PM image of an activity recording site in an awake, GCaMP6s-expressing transgenic mouse (*CamKII-tTa/tetO-GCaMP6s*, male, 15 weeks old). The recording site is 600 mm below the brain surface with a scanning field of ~3.23 mm x 3.23 mm. Panels 1-5 show digitally zoomed-in images from the corresponding white dashed boxes in **a**. Scale bar: 1 mm. Scale bars in panels 1 to 5: 100 mm. (**b)** Spontaneous activity traces recorded under awake conditions from 918 neurons in **a**. The average power on the brain surface was 119 mW. 53% of the scanned area was excited using the adaptive excitation scheme. The recordings were acquired with 1030x1030 pixels per frame, with a pixel size of 3.14 mm and a frame rate of 4.0 Hz using two beamlets and the polygon scanner. **(c)** Selected activity traces from **b**. **(d)** Images of six focal planes acquired simultaneously by 1320 nm 3PM (green) and 920 nm 2PM (yellow) in an awake, GCaMP6s-expressing transgenic mouse (*CamKII-tTa/tetO-GCaMP6s*, female, 17-weeks old). The activity recording sites were 320, 340, 360, 380, 400 and 600 mm below the brain surface with a scanning field of ~3.23 x 3.23 mm. Scale bar, 1 mm. Panels 1 and 2 show digitally zoomed-in images from the corresponding white dashed boxes. Scale bar, 100 mm. **(e)** Spontaneous activity traces recorded by 920 nm 2PM under awake conditions from 4183 neurons (total from the five focal planes) in the FOV in **d**. **(f)** Selected activity traces from **e**. (**g)** Spontaneous activity traces recorded by 1320 nm 3PM under awake conditions from 340 neurons in the FOV in **d**. **(h)** Selected activity traces from **g**. For 3P imaging, the average power on the brain surface was 97 mW. 46% of the scanned area was excited using the adaptive excitation scheme. The recordings were acquired with 1030x1030 pixels per frame, a pixel size of 3.14 mm and a frame rate of 11 Hz using two beamlets. For 2P imaging, the laser repetition rate used for imaging was 80 MHz, and the average power on the brain surface was 75 mW. 62% of the scanned area was excited using the adaptive excitation scheme. The recordings were acquired with 1030 x 515 pixels per frame, a pixel size of 3.14 x 6.28 mm and a volume rate (i.e., the cycling rate among the five focal planes) of 2.2 Hz.